

ON MICRO-DAMAGE IN HOT METAL WORKING
PART 2: CONSTITUTIVE MODELLING

J. Lin¹⁾, A.D. Foster¹⁾, Y. Liu¹⁾
D.C.J. Farrugia²⁾, T.A. Dean¹⁾

¹⁾Department of Manufacturing and Mechanical Engineering
School of Engineering
University of Birmingham
Edgbaston, Birmingham B15 2TT, UK

²⁾Corus R, D and T, Swinden Technology Centre
Moorgate, Rotherham, S60 3AR, UK

Damage constitutive equations are formulated to model the evolution of grain boundary and plasticity-induced damage for free-cutting steels under hot forming conditions. During high temperature, high strain rate deformation, material degradation has characteristics of both creep damage at grain boundaries, and ductile damage surrounding hard inclusions. This has been experimentally observed and is reported in the companion paper. This paper describes the development of unified viscoplastic-damage constitutive equations, in which the nucleation and growth of both damage types are considered independently. The effects of deformation rate, temperature, and material microstructure on damage evolution are modelled. The proposed damage evolution equations are combined with a viscoplastic constitutive equation set, enabling the evolution of dislocation hardening, recovery, recrystallisation, grain size, and damage to be modelled. This set of unified, mechanism-based, viscoplastic damage constitutive equations is determined from experimental data of a free-machining steel for the temperature range 1173–1373 K. The fitted model is then used to predict damage and failure features of the same material tested using a set of interrupted constant strain rate tests. Close agreement between the predicted and experimental results is obtained for all the cases studied.

Key words: creep damage, ductile damage, constitutive equations, hot metal forming, viscoplasticity.

NOTATIONS

ε_p	plastic strain,
ε_T	total strain,
A_1, A_2, γ_1	material constants in plastic strain rate law,
d	average grain size,
d_0	material constant for grain size dependence,
R	isotropic hardening parameter,
k	material yield stress,

S	recrystallised fraction,
$\bar{\rho}$	normalised dislocation density,
$\bar{\rho}_c$	material-dependent critical dislocation density for recrystallisation,
x	recrystallisation onset parameter,
H_1, λ_1	material constants in recrystallisation law,
δ_1, δ_2	material constants in dislocation accumulation law,
C_r, δ_3	material constants in dislocation recovery law,
C_S	material constant in dislocation annihilation by recrystallisation law,
X_1	material constant in recrystallisation onset law,
B	material constant in isotropic hardening law,
G_1, ψ_1	material constants in normal grain growth law,
G_2, ψ_2	material constants in grain size evolution law,
E	Young's modulus of material,
σ	residual stress,
D_T	total damage,
D_{GB}	grain boundary damage,
D_{GB}^N, D_{GB}^G	grain boundary damage nucleation and growth,
η	grain size dependence parameter for grain boundary damage,
d_c	critical grain size parameter for grain boundary damage,
a_1, a_2, a_3, n_1	material constants in grain boundary damage accumulation law,
a_4	material constant in grain boundary damage nucleation law,
n_2	material constant in grain boundary damage growth law,
D_{Pi}	plasticity-induced damage,
D_{Pi}^N, D_{Pi}^G	plasticity-induced damage nucleation and growth,
a_5	material constant in plasticity-induced damage accumulation law,
a_6, n_3, n_4	material constants in plasticity-induced damage growth law,
Q_p, Q_{ac}, Q_{GG}	activation energy for i) dislocation-based plasticity, ii) dislocation recovery, iii) grain growth,
Q_{GB}, Q_{Pi}	activation energy for i) grain boundary damage, ii) plasticity induced damage,
κ, T	heat constant, temperature.

1. INTRODUCTION

Damage modelling is now recognised as a powerful tool for the understanding and prediction of the initiation of macro-cracks in materials processing. Hot metal forming processes inadvertently cause a concentrated build-up of micro-damage within the working material at areas, where hydrostatic stress is positive [1]. It is the accumulation of this damage that can cause macro-cracking observed on feedstock during rolling. Macroscopic cracks are formed when micro-damage features reach a critical density and start to coalesce. In commercial rolled steels, a uniform, high-quality product is essential. To achieve this, regions with a high damage density are removed, a process which is expensive and wasteful. By using a damage model to accurately determine the critically damaged region, yield can be increased and specified mechanical properties of processed materials achieved. To enable the grain boundary damage and plasticity-induced damage observed from experimentation of hot metal working conditions to be

modelled, relevant damage models for high temperature creep, plasticity and superplasticity are outlined first.

Since the original work on damage accumulation during high temperature creep by KACHANOV [2], continuum damage mechanics (CDM) has been applied to a range of deformation conditions. For the case of high temperature creep in which viscoplastic straining occurs predominantly by grain boundary sliding due to the grain boundary diffusion process, damage has been identified as occurring by several damage mechanisms, with the dominant mechanism depending on both the material and the strain rate. The damage types have been independently studied and modelled, for instance damage due to mobile dislocations in creep has been modelled by using the equation form [3]:

$$(1.1) \quad \dot{D} = C (1 - D)^2 \dot{\varepsilon}_c$$

in which D represents damage in a unit area (varying from an undamaged state of $D = 0$ to a totally damaged state at $D = 1$), $\dot{\varepsilon}_c$ is the creep strain rate, and C is a material constant. Damage due to creep constrained cavity nucleation and growth (occurring at grain boundaries) is typically represented by

$$(1.2) \quad \dot{D} = W \dot{\varepsilon}_c,$$

where W is a material constant [4]. If high temperature creep takes place under high stress levels, cavity growth is the dominant damage mechanism. According to COCKS and ASHBY [5], damage due to cavity growth at grain boundaries is modelled by

$$(1.3) \quad \dot{D} = \beta \left(\frac{1}{(1 - D)^n} - (1 - D) \right) \left(\frac{\sigma_e}{\sigma_0} \right) \cdot \dot{\varepsilon}_0$$

in which σ_0 and n denote material constants, $\dot{\varepsilon}_0$ is the material creep rate, and β is a material parameter related to hydrostatic stress.

Deformation at low temperatures occurs predominantly by the formation and slip of dislocations within grains. Under these conditions, ductile damage nucleates and grows around the second phase and other matrix discontinuities that attract a localised build up of dislocations. Detailed studies of ductile void growth have been conducted by RICE and TRACEY [6] and GURSON [1]. RICE and TRACEY [6] proposed a damage model based on the radial growth characteristics of a pre-existing void in a unit cell, considering in detail the volumetric growth and shape changes of a void. Later, Gurson's approximation of a rigid-plastic solid containing spherical cavities [1] considered the micro-effects of a growing void within a continuum lattice. The model gives a good representation of the early evolution of damage, however coalescence is presumed as being

solely due to adjacent cavities meeting – which leads to a large discrepancy between the predicted and actual failure conditions [7]. Phenomenologically based ductile damage models have also been developed to model the damage accumulation due to large plastic deformation. By considering void nucleation and growth as separate terms, damage can be represented by the form [8]:

$$(1.4) \quad \dot{D} = c \cdot \dot{\varepsilon}_e^p + (a_1 + a_2 \cdot D) \cdot \frac{K^2}{2E} \cdot (\varepsilon_e^p)^{2m} \cdot f\left(\frac{\sigma_H}{\sigma_e}\right) \cdot \dot{\varepsilon}_e^p$$

in which c, a_1 , and a_2 are material-dependant constants, and K and m are hardening parameters. The first term represents the rate of nucleation of new damage sites, the second models the growth of existing voids. The function $f\left(\frac{\sigma_H}{\sigma_e}\right)$ describes the stress state dependence of void growth.

Damage accumulation during superplastic deformation has been identified at grain boundaries [9] and around hard particles both at grain boundaries and within grains [10]. A damage model to predict damage during superplastic deformation occurring by void nucleation and growth around particles has been developed by KHALEEL [10] and takes the form:

$$(1.5) \quad \dot{D} = \eta \cdot (1 - D) \cdot \dot{\varepsilon}_p + \frac{F(\varepsilon_p)}{(1 - D)} \cdot \sigma \cdot \dot{\varepsilon}_p,$$

where η is usually taken as a material constant and F is a monotonic function of plastic strain.

The models discussed above are designed to predict particular types of damage evolution and damage mechanisms. In the companion paper, an experimental programme conducted on a free-cutting steel has identified the simultaneous presence of two discrete types of damage. Cracks and voids along grain boundaries and at triple points of adjacent grains (referred to as grain boundary damage in this paper) have similarities to those noted during high temperature creep (e.g. [11]) and superplastic deformation. Damage surrounding hard inclusions due to debonding of the inclusion/matrix interface is similar to a damage example considered by GURSON [1] and others in ductile rupture conditions, as well as that modelled by KHALEEL [10] for superplastic deformation. The rate of accumulation of each damage type is affected by temperature, strain rate, and material (especially the presence of hard inclusions within the material), but the two damage types react very differently to a change in deformation conditions or material. In addition, many dynamic matrix-reorganisation processes also affect damage development such as hardening by dislocation accumulation, subsequent softening by recovery and recrystallisation processes, grain size reduction by recrystallisation, and normal grain growth. The main aim of this paper

is to produce a damage model for hot deformation that is capable of following the evolution and the macroscopic effect of the two damage types encountered during uniaxial experimental testing.

The work presented in this paper concentrates on the identification of interactions between the mechanisms of hot deformation and the accumulation of the two damage types described above. A phenomenological model for grain boundary and plasticity-induced damage is built and, by coupling this with a modified version of LIN and LIU's model for microstructure evolution in hot deformation [12], a complete set of viscoplastic-damage constitutive equations is presented. The constants within the viscoplastic damage constitutive equations are determined for a free-cutting steel over the temperature range of 1173–1373 K and deformation rates of 0.1–10 s⁻¹. The model is then used to predict the material flow stress evolution of a set of interrupted constant strain rate tests, and compared with experimental results.

2. DEVELOPMENT OF DAMAGE MODELS

The response of the two damage mechanisms to factors such as temperature, strain rate and grain size are not similar, and thus an independent mechanism is assigned for each damage type. Damage accumulation is considered as being homogeneous, and is treated as a phenomenological continuum model for simple tension in the present work.

2.1. Damage equation set

The two damage mechanisms independently map the accumulation of each damage type. Material failure is determined by the total damage, defined as the sum of both damage types. Total damage is initially 0 representing the undamaged state, and rises to a value of 0.9 at which point damage coalesces and macrocracks develop, which is the criteria for material failure. The total damage D_T is in the form:

$$(2.1) \quad D_T = D_{GB} + D_{Pi} \quad (D_T < 0.9).$$

Damage is accumulated by the nucleation of new damage sites and the growth of pre-existing sites, thus the grain boundary damage, D_{GB} , and plasticity-induced damage, D_{Pi} , are represented as:

$$(2.2) \quad \dot{D}_{GB} = \dot{D}_{GB}^N + \dot{D}_{GB}^G,$$

$$(2.3) \quad \dot{D}_{Pi} = \dot{D}_{Pi}^N + \dot{D}_{Pi}^G$$

in which \dot{D}_{GB}^N and \dot{D}_{GB}^G are the rates of nucleation and growth of damage at grain boundaries, \dot{D}_{Pi}^N and \dot{D}_{Pi}^G are the rates of nucleation and growth of plasticity-induced damage.

The accumulation rate of grain boundary damage is highly dependent on the grain size. If grains are large, there is less grain boundary sliding and grain rotations under hot-deformation conditions and damage accumulation at grain boundaries is slow. If grain size is very small ($<10 \mu\text{m}$), superplasticity is achieved, grains can rotate and slide past each other with ease and damage accumulation is again slow. A grain size between these two extremes will cause the highest grain boundary damage accumulation rate. In addition, the band of critical grain size is dependent of deformation rate (Fig. 1). Fast deformation favours dislocation-based plastic deformation, meaning that the grain size to achieve grain boundary movement is relatively smaller, and superplasticity is not easily achieved. In contrast, slow deformation favours grain boundary sliding due to grain-boundary diffusion, and so the critical grain size becomes larger. To reflect this, the equation to describe grain boundary damage accumulation has been modified to reflect grain size, strain rate, as well as temperature-dependence and is given by:

$$(2.4) \quad \dot{D}_{GB} = \eta \cdot (\dot{D}_{GB}^N + \dot{D}_{GB}^G)$$

in which the damage compliance variable, η , is defined as:

$$(2.5) \quad \eta = a_1 \cdot \exp \left(-a_2 \cdot \left(1 - \frac{d}{d_c} \right)^2 \right),$$

$$(2.6) \quad d_c = a_3 \cdot (\dot{\varepsilon}_p)^{-n_1},$$

where a_1 , a_2 , a_3 and n_1 are constants. The characteristic curves of the compliance variable η are given in Fig. 1 with variations of grain size for different deformation rates. For these calculations the values of constants are as given in Table 2. Equation (2.6) calculates the critical grain size for which grain boundary damage accumulation is at a maximum, which is a function of strain rate. Equation (2.5) reduces the accumulation rate when the actual grain size is not at the critical value. The highest grain boundary damage accumulation rate varies with grain size and strain rates [Fig. 1].

Nucleation of grain boundary damage is encouraged when grains are harder than the grain boundaries, leading to plastic deformation by grain boundary movement, thus the damage nucleation variable is strongly influenced by dislocation density (intra-grain hardness):

$$(2.7) \quad \dot{D}_{GB}^N = a_4 \cdot (1 - D_{GB}) \cdot \dot{\rho}$$

in which a_4 is a material constant.

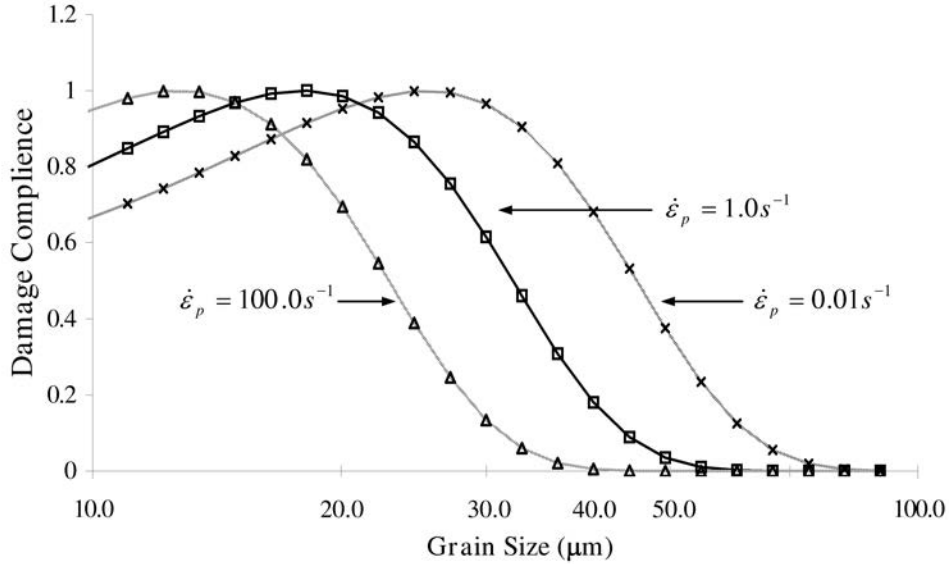


FIG. 1. Grain boundary damage compliance plotted against grain size for $T = 1273$ K.

Grain boundary damage grows so long as plastic deformation is taking place. COCKS and ASHBY [4] proposed an equation for the strain-controlled void growth of creep damage; modified for the present work, the equation takes the form:

$$(2.8) \quad \dot{D}_{GB}^G = \left[\frac{1}{(1 - D_{GB})^{n_2}} - (1 - D_{GB}) \right] \cdot \dot{\varepsilon}_p,$$

where n_2 is a constant. Plasticity-induced damage is created by the accumulation of dislocations around a hard inclusion. The nucleation of plasticity-induced damage is thus directly related to the amount of dislocation-based deformation experienced by the grain structure. A further consequence of this is that any softening processes acting to reduce the density of dislocations will also have a stabilising effect on nucleated voids. Using a similar term to that given in (1.1), but substituting creep strain rate for dislocation evolution rate, the rate of nucleation of plasticity-induced damage can be represented by:

$$(2.9) \quad \dot{D}_{Pi}^N = (1 - D_{Pi}) \cdot \dot{\rho}.$$

The growth rate of plasticity-induced damage is a function of grain size, strain rate, and temperature, along with the amount of plasticity-induced damage that has been created. A large grain size favours deformation by dislocation movement and thus increases the rate of accumulation of plasticity-induced damage. For

the same reason, high strain rates increase the growth rate of plasticity-induced damage. The modelling equation is given as:

$$(2.10) \quad \dot{D}_{Pi}^G = a_6 d \frac{D_{Pi}}{(1 - D_{Pi})^{n_3}} \cdot |\dot{\varepsilon}_p|^{n_4},$$

where a_6 , n_3 and n_4 are constants.

2.2. Modelling the effect of damage on viscoplastic deformation

The basic model used for plastic strain is a hyperbolic sine law, with hardening and grain size effects considered [12], of the form:

$$(2.11) \quad \dot{\varepsilon}_p = \frac{A_1 \cdot \sinh [A_2 \cdot (\sigma - R - k)]}{d^{\gamma_1}},$$

where A_1 , A_2 , and γ_1 are material constants. k is the initial yield stress of the material and R is the isotropic hardening due to plastic deformation. γ_1 characterises the effect of grain size on the viscoplastic flow of the material.

Damage at grain boundaries reduces the load bearing section over which a deformation force acts. This increases the effective stress according to the common practice of dealing with creep damage. Plasticity-induced damage is considered in much the same way; voids growing within grains will distribute and focus flow stress away from the voids [7]. The localisation of stress into the lattice generates more force to overcome grain hardening, when viewed from outside the grain, this leads to a softer grain that is easier to deform. In other words, plasticity-induced damage shrinks the yield surface of the material. Thus considering the softening effects due to damage, Eq. (2.11) is written as:

$$(2.12) \quad \dot{\varepsilon}_p = A_1 \cdot \sinh \left[A_2 \cdot \left(\frac{\sigma}{(1 - D_{GB})} - (R + k) \cdot (1 - D_{Pi}) \right) \right] d^{-\gamma_1}$$

in which grain boundary damage increases the effective stress causing plastic deformation, and plasticity-induced damage decreases the effective material hardness.

3. DEVELOPMENT OF UNIFIED VISCOPLASTIC-DAMAGE CONSTITUTIVE EQUATIONS

Unified constitutive equations for viscoplasticity have been developed for many metal materials [13, 14]. The equations enable a wide range of time-dependent phenomena to be modelled, such as strain hardening, stress relaxation and ratchetting [15], and in addition enable the important time-dependent

effects, such as strain rates, recovery and creep to be modelled. This work intends to develop a set of unified viscoplastic damage constitutive equations to model the evolution of recrystallisation, dislocation density, hardening and grain size, damage at grain boundaries and around the second phase particles, to rationalise their inter-relationships and effects on viscoplastic flow of materials. The mechanism-based unified viscoplastic damage constitutive equations for hot metal forming may take the form:

$$(3.1) \quad \dot{\varepsilon}_p = A_1 \cdot \sinh \left[A_2 \cdot \left(\frac{\sigma}{1 - D_{GB}} - (R + k) \cdot (1 - D_{Pi}) \right) \right] \left(\frac{d}{d_0} \right)^{-\gamma_1},$$

$$(3.2) \quad \dot{S} = H_1 \cdot (x \cdot \bar{\rho} - \bar{\rho}_c \cdot (1 - S)) \cdot (1 - S)^{\lambda_1},$$

$$(3.3) \quad \dot{x} = X_1 \cdot (1 - x) \cdot \bar{\rho},$$

$$(3.4) \quad \dot{\bar{\rho}} = \left(\frac{d}{d_0} \right)^{\delta_1} \cdot (1 - \bar{\rho}) \cdot |\dot{\varepsilon}_p|^{\delta_2} - C_r \cdot \bar{\rho}^{\delta_3} - \frac{C_S \cdot \bar{\rho}}{1 - S} \dot{S},$$

$$(3.5) \quad \dot{R} = 0.5 \cdot B \cdot \bar{\rho}^{-1/2} \cdot \dot{\bar{\rho}},$$

$$(3.6) \quad \dot{d} = \left(\frac{G_1}{d} \right)^{\psi_1} - G_2 \cdot \dot{S} \cdot \left(\frac{d}{d_0} \right)^{\psi_2},$$

$$(3.7) \quad \sigma = E \cdot (\varepsilon_T - \varepsilon_p),$$

$$(3.8) \quad \dot{D}_{GB} = \eta \cdot \left([a_4 \cdot (1 - D_{GB}) \cdot \dot{\bar{\rho}}] + \left[\left(\frac{1}{(1 - D_{GB})^{n_2}} - (1 - D_{GB}) \right) \cdot |\dot{\varepsilon}_p| \right] \right),$$

$$(3.9) \quad \dot{D}_{Pi} = a_5 \cdot \left([(1 - D_{Pi}) \cdot \dot{\bar{\rho}}] + \left[a_6 \cdot \frac{D_{Pi} \cdot d}{(1 - D_{Pi})^{n_3}} \cdot |\dot{\varepsilon}_p|^{n_4} \right] \right),$$

$$(3.10) \quad \dot{D}_T = \dot{D}_{GB} + \dot{D}_{Pi}.$$

Grain boundary damage parameter η has been defined in Eq. (2.5). Temperature-dependent material parameters in the Eqs. (3.1)–(3.10) are defined in Table 1.

Viscoplastic flow of the material is modelled using Eq. (3.1), which is a function of flow stress, σ , grain boundary damage, D_{GB} , plasticity-induced damage, D_{Pi} , isotropic hardening, R , and the average grain size, d . Equation (3.2) models the volume fraction of recrystallised grains during and after hot deformation. The incubation time for recrystallisation is controlled by Eq. (3.3), which is directly related to the accumulation of normalised dislocation density. The volume

Table 1. Temperature-dependent parameters.

$k = k_{(0)} \cdot \exp\left(\frac{Q_p}{\kappa \cdot T}\right)$	$\bar{\rho}_c = \bar{\rho}_{c(0)} \cdot \exp\left(\frac{Q_p}{\kappa \cdot T}\right)$
$C_r = C_{r(0)} \cdot \exp\left(\frac{-Q_{ac}}{\kappa \cdot T}\right)$	$X_1 = X_{1(0)} \cdot \exp\left(\frac{-Q_{ac}}{\kappa \cdot T}\right)$
$G_1 = G_{1(0)} \cdot \exp\left(\frac{-Q_{GG}}{\kappa \cdot T}\right)$	$E = \frac{E_{(\text{ref})}}{\cosh^2(K_1 \cdot (T - T_{(\text{ref})}))}$
$\alpha_1 = \alpha_{1(0)} \cdot \exp\left(\frac{Q_{GB}}{\kappa \cdot T}\right)$	$\alpha_5 = \alpha_{5(0)} \cdot \exp\left(\frac{Q_{Pi}}{\kappa \cdot T}\right)$

fraction of recrystallisation variable, S , varies from 0 (no recrystallised grains) to 1.0 (representing the fully recrystallised state).

The normalised dislocation density is defined by $\bar{\rho} = (\rho - \rho_i)/\rho$, where ρ is the current dislocation density and ρ_i is the dislocation density for the virgin material. When the plastic deformation is high, $\rho \gg \rho_i$. Thus the range of normalised dislocation density varies from 0 to 1.0. Equation (3.4) models the evolution of the normalised dislocation density. The first term in the equation models the accumulation of dislocations due to viscoplastic deformation $|\dot{\varepsilon}_p|$ and the dynamic recovery of the dislocation density. The second term in the equation represents the annealing process, which reduces the dislocation density. Recrystallisation creates dislocation free grains, which results in the reduction of average dislocation density. The evolution of the normalised dislocation density due to recrystallisation is described by the third term of Eq. (3.4). The hardening of the material due to plastic deformation is directly related to the dislocation density and its evolution is given by Eq. (3.5). The effects of grain size on the accumulation of dislocation density is controlled by $(d/d_0)^{\delta_1}$. Small grain size facilitates the grain boundary sliding and grain rotation under viscoplastic deformation. Thus less strain is ‘carried by dislocations’. The average grain size evolution is described by Eq. (3.6). The first term of the equation represents the static grain growth and the second the grain refinement due to recrystallisation. Flow stress is calculated from the elastic strain in the usual way; Eq. (3.7) along with details of the above viscoplastic constitutive equations are given by LIN *et al.* [12].

The grain boundary damage evolution is represented by Eq. (3.8). The effects of grain size and strain rates on grain boundary damage evolution are controlled by the parameter η (Eqs. (2.5) and (2.6)). Nucleation and growth rates of plasticity-induced damage are described by Eq. (3.9), which is directly related to Eqs. (2.3), (2.9) and (2.10). The total damage evolution is given by Eq. (3.10). The material constants, as indicated by the nomenclature and given

in Table 2, are determined from experimental data using an Evolutionary Programming (EP)-based optimisation technique developed by LI *et al.* [16] using the objective function detailed by LIN *et al.* [17]. The details of the optimisation process and the numerical procedure for this type of the problems are described by LIN *et al.* [12] and LI *et al.* [16].

Table 2. Material constants for the free-cutting steel.

Constant	Determined Value	Constant	Determined Value
A_1	(s^{-1}) 68.0	κ	($J \cdot mol^{-1} \cdot K^{-1}$) 8.31
A_2	(MPa^{-1}) 1.5e-2	Q_p	($J \cdot mol^{-1}$) 1.069e5
γ_1	(–) 1.0	Q_{ac}	($J \cdot mol^{-1}$) 4.082e5
$k_{(0)}$	(MPa) 6.81e-4	$E_{(ref)}$	(MPa) 1.27e5
H_1	(s^{-1}) 14.5	K_1	(K^{-1}) 2.0e-3
$\bar{\rho}_{c(0)}$	(–) 1.10e-7	$T_{(ref)}$	(K) 1073
λ_1	(–) 1.0	$\alpha_{1(0)}$	(–) 1.3e-4
d_0	(μm) 28.67	α_2	(–) 1.1
δ_1	(–) 1.02	α_3	(μm) 18.0
δ_2	(–) 1.5	n_1	(–) 7.5e-2
$C_{r(0)}$	(s^{-1}) 1.13e17	α_4	(–) 3.8e-5
δ_3	(–) 2.13	n_2	(–) 4.66
C_S	(–) 1.0	$\alpha_{5(0)}$	(–) 2.04e-3
$X_{1(0)}$	(s^{-1}) 1.44e17	α_6	(μm^{-1}) 2.33
B	(MPa) 1.60e2	n_3	(–) 14.0
$G_{1(0)}$	(μm) 6.401e4	n_4	(–) 0.89
ψ_1	(–) 0.875	Q_{GG}	($J \cdot mol^{-1}$) 7.020e4
G_2	(s^{-1}) 26.61	Q_{GB}	($J \cdot mol^{-1}$) 1.017e5
ψ_2	(–) 0.90	Q_{Pi}	($J \cdot mol^{-1}$) 2.5e4

4. MODELLING RESULTS AND EXPERIMENTAL VALIDATION

4.1. Experimental results for the determination of material parameters

Hot uniaxial tensile tests were performed to obtain the stress-strain relationships for a range of constant strain rates and temperatures, which are used in the determination of material constants within the equations. The experimental programme was conducted on a Gleeble material simulator using a free-cutting steel which contained hard manganese sulphide inclusions, evenly distributed through the grain structure in the tested temperature range. The experimental programme was identical to that described in detail in the companion paper for a free-cutting steel. A 5-minute soaking process performed at 1473 K was

used to create a uniform microstructure, after which constant strain rate tests were conducted at strain rates between $0.1\text{--}10\text{ s}^{-1}$ at a temperature of 1273 K, and at a strain rate of 1.0 s^{-1} at temperatures between 1173 and 1373 K. The determined material constants are listed in Table 2.

Figure 2 shows experimental data plotted alongside the stress-strain curves generated by the fitted equation set for a range of strain rates and temperatures. The fitted model is consistent with test results, displaying good accuracy in the prediction of flow stresses as well as strains at failure for all conditions given, with strains at failure showing less than 5% discrepancy in all conditions. The peak in flow stress followed by an extended ductility that is associated with dynamic recrystallisation is prominent in low strain rate and high temperature stress-

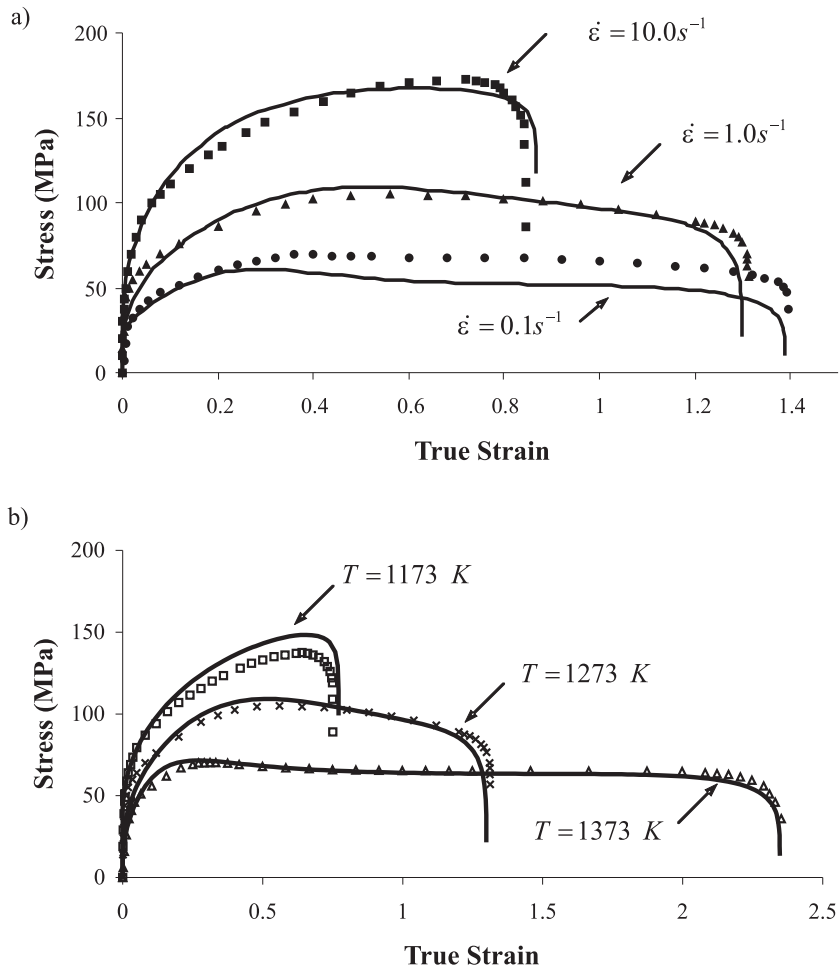


FIG. 2. Comparison of experimental (symbols) and computed (curves) stress-strain relationships for (a) different strain rates at 1273 K and (b) different temperatures at $\dot{\varepsilon} = 1.0\text{ s}^{-1}$.

strain plots, becoming less prominent with increasing strain rate and decreasing temperature.

It is understood that for high temperature, small grain size and low strain-rate deformation conditions, the dominant deformation mechanism is through grain boundary sliding and grain rotation. This results in inter-granular failure due to the accumulation of grain boundary damage. If the deformation rate is high, the grain size large and temperature is low, the strain is mainly carried by dislocations and voids at inclusions can be observed. This is due to the ac-

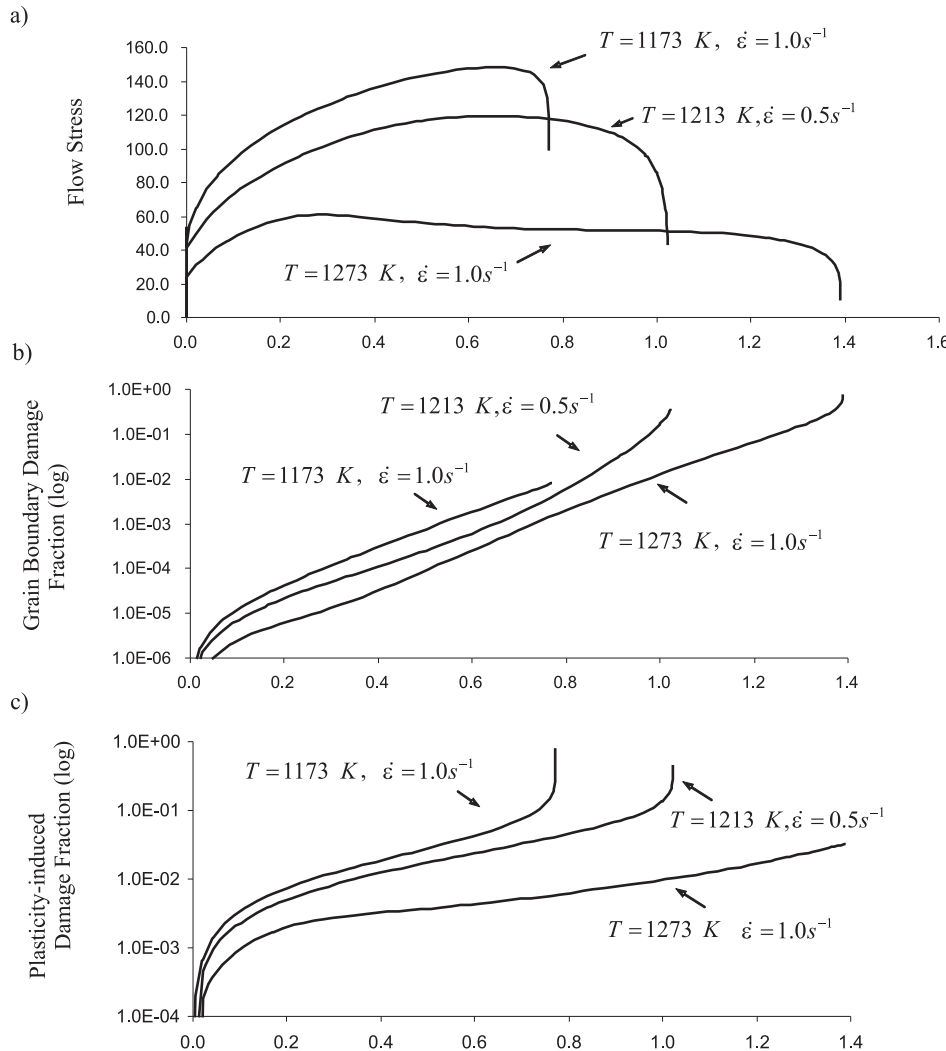


FIG. 3. Change of dominant damage type with increasing strain rate: a) flow stress plot for 3 deformation conditions, b) grain boundary damage, c) plasticity-induced damage.

cumulation of plasticity-induced damage. Calculations were carried out using the determined viscoplastic damage constitutive equations with the same initial grain size, different temperature and strain rates. Figure 3 shows the predicted results for flow stress (a), grain boundary damage (b), and plasticity-induced damage (c), for three loading conditions. are: (i) Low temperature and high strain rate: $T = 1173\text{ K}$ and $\dot{\varepsilon}_T = 1.0\text{ s}^{-1}$; (ii) Medium temperature and strain rate: $T = 1213\text{ K}$ and $\dot{\varepsilon}_T = 0.5\text{ s}^{-1}$; and, (iii) High temperature and low strain rate: $T = 1273\text{ K}$ and $\dot{\varepsilon}_T = 0.1\text{ s}^{-1}$. When the total damage reaches 0.9, the failure takes place. Figure 3 shows that, for the first case, plasticity-induced damage is dominant over grain boundary damage. As the deformation temperature increases and strain rate decreases, the balance damage state can be observed. However, when the temperature increases further, grain boundary sliding deformation mechanism plays more important role. This results in a high value of grain boundary damage.

4.2. Experimental and modelled results of interrupted deformation tests

A second test set was conducted using an interrupted deformation programme. The testpieces were soaked for 5 minutes at 1473 K and then deformed at a total strain rate of 10 s^{-1} and a temperature of 1273 K. On reaching a pre-specified strain, the test was interrupted. Deformation was halted and testpiece temperature was maintained. During the interrupt period, metadynamic recovery processes develop, simulating the microstructure development between successive passes of a multi-pass hot-rolling schedule. Interruptions lasting 0.3–10 s were imposed once a true strain of 0.3 had been reached, corresponding with a point in deformation at which recrystallisation nucleations are present, but dynamic recrystallisation (DRX) is not apparent. Once the desired interrupt time is reached, the testpiece deformation was continued to failure.

The test programme was modelled using the developed equation set by emulating the physical restrictions given in the tests. The model was started with conditions of $\dot{\varepsilon}_T = 10\text{ s}^{-1}$ and $T = 1273\text{ K}$. On reaching a strain $\varepsilon_T = 0.3$, the conditions of the model were forced to $\dot{\varepsilon}_p, \dot{\varepsilon}_T = 0\text{ s}^{-1}$. All other mechanisms and conditions were left unrestrained, resulting in the metadynamic reorganisation processes such as recovery and recrystallisation continuing to evolve, emulating the material evolution in the test programme. After the predefined interrupt time had passed, the model conditions were returned to $\dot{\varepsilon}_T = 10\text{ s}^{-1}$ and deformation continued as before, until the termination condition of damage coalescence was reached.

The simulation of interrupted constant strain rate tests shows promising results. Stress-strain plots correctly predict the general shape of the curves (Fig. 4). The general trend exhibited by the strain at failure following reload-

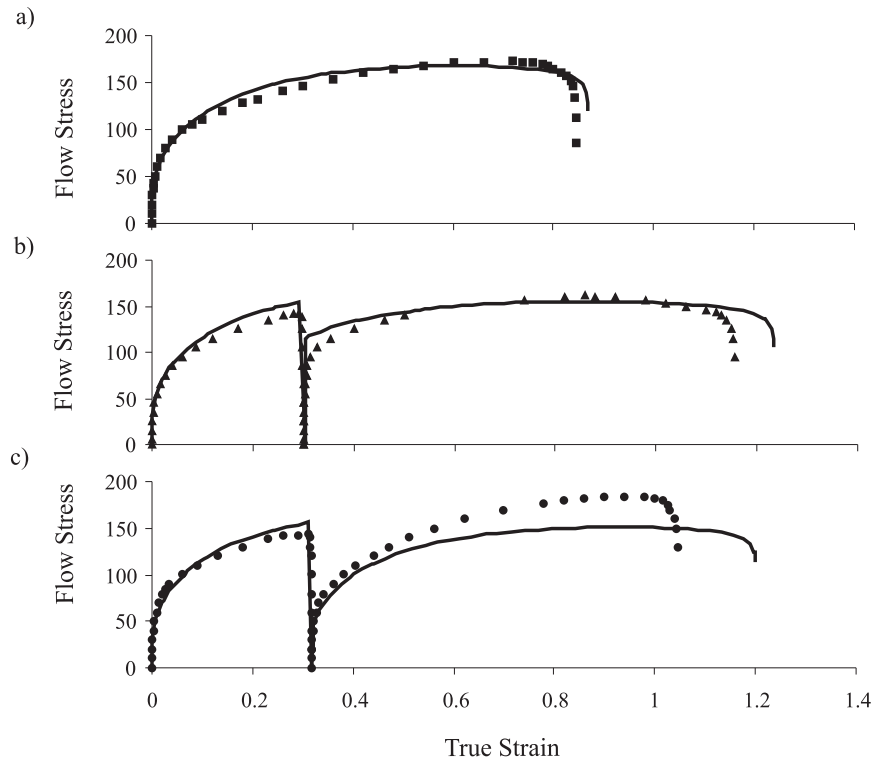


FIG. 4. Comparison of experimental (symbol) and computed (curves) interrupted flow stress curves at $\dot{\varepsilon} = 10 \text{ s}^{-1}$ and $T = 1273 \text{ K}$ for interrupt periods of (a) 0.0 s, (b) 0.3 s, and (c) 5.0 s.

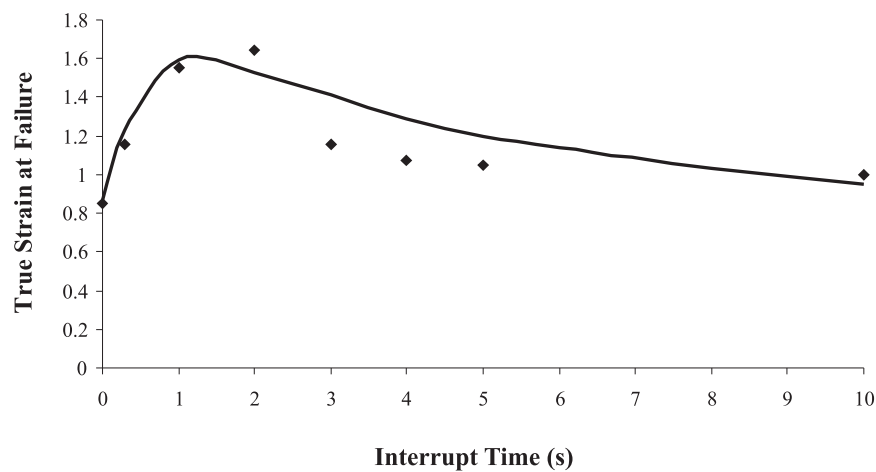


FIG. 5. Comparison of experimental (symbols) and computed (curve) strain at failure against interrupt period for $\dot{\varepsilon} = 10 \text{ s}^{-1}$ and $T = 1273 \text{ K}$.

ing is correctly predicted (Fig. 5), with the predicted interrupt time leading to maximum ductility falling only marginally short of the experimentally determined value. The complex relationship between the interrupt period and the resulting reloading curve is interpreted within the model as the result of grain size and dislocation density changes resulting from metadynamic recovery, recrystallisation (MDRX), and grain size changes. A detailed explanation of the test results can be formed by splitting the material evolution into a number of stages.

Stage 1: Strain is applied at a constant strain rate. As the testpiece is strained, recrystallisation nucleation sites may develop within the material. No significant amount of DRX occurs. At a constant strain rate of 10 s^{-1} , this stage will last approximately 0.03 s, during which no notable grain growth occurs.

Stage 2: Interrupt strain is reached. Deformation is stopped. Recrystallisation may continue depending on the remaining dislocation density, which reduces due to recrystallisation and annealing effects. Grain refinement takes place due to recrystallisation. Nucleated MDRX grains grow within the lattice until the new grain recrystallisation fronts meet. During this period, a limited amount of damage recovery takes place due to the reduction of dislocation density. Normal grain growth occurs depending on the interrupted intervals. Complex microstructure evolution takes place during inter-passes.

Stage 3: Constant strain rate deformation is restarted. Material evolution this point depending on what stage was reached before deformation was continued.

The interrupted tests were used to give an indirect measurement of the material's RX characteristics. By interpreting the interrupted flow stress results it has been possible to identify the relationship between the completeness of RX and material flow response. This relationship is critical if the model is to remain accurate in complex RX conditions; the model's accuracy can be improved by collecting additional experimental data to directly fit the data for static RX or grain size evolution.

In the companion paper, it has been discussed that recrystallisation processes may annihilate or reduce damage nucleations and young (physically small) damage sites. The damage level within the proposed model is reduced by the dislocation-linked reduction in damage nucleation sites; both of plasticity-induced and grain boundary damage.

The current model is not capable of accurately predicting the peak flow stress following reloading, which is predicted as varying only slightly with interrupt time, suggesting that further development of grain size and hardening mechanisms are required to improve the accuracy. The comparison of experimental and peak flow stress for the reloading state can be observed in Fig. 4. The trend

of the strain at failure for the reloading stage can be also predicted using the equation set, although the highest error is about 15% between the experimental and predicted results, which are shown in Fig. 5.

5. CONCLUSIONS

A set of unified viscoplastic damage constitutive equations has been formulated and determined to model the damage evolution features observed in experiments for a free-cutting steel under hot working conditions. In addition to recrystallisation, grain size evolution and dislocation hardening, the effects of microstructure, strain rates and temperature on the grain boundary damage and plasticity-induced damage can be predicted. The developed constitutive equation set can also be used to model the viscoplastic flow, microstructure evolution and failure of the material under interrupted loading conditions, including the microstructural evolution during the interval of the loadings. The errors of the prediction are within 20% for peak flow stress and 15% for strains at failure.

ACKNOWLEDGMENTS

The financial support provided by Corus UK Ltd for both Y. Liu and A. D. Foster is gratefully acknowledged.

REFERENCES

1. A.L. GURSON, *Continuum theory of ductile rupture by void nucleation and growth: Part 1 – Yield Criteria and Flow Rules for Porous Ductile Media*, J. Engng. Matr. Tech., **99**, 1977.
2. L.M. KACHANOV, *Time to the rupture process under creep conditions*, Izv. Akad. SSR. Oid. Tekh. Nauk., **8**, 26–31, 1958.
3. J. LIN, D.R. HAYHURST, and B.F. DYSON, *The standard ridges uniaxial creep testpiece: computed accuracy of creep strain*, J. of Strain Analysis, **28**, 2, 101–115, 1993.
4. B.F. DYSON, *Creep and fracture of metals: mechanisms and mechanics*, Revue Phys. Appl., **23**, 605–613, 1988.
5. A.C.F. COCKS and M.F. ASHBY, *On creep fracture by void growth*, Progress in Material Science, **27**, 189–244, 1982.
6. J.R. RICE and D.M. TRACEY, *On the ductile enlargement of voids in triaxial stress fields*, J. of the Mechanics and Physics of Solids, **17**, 201–217, 1969.
7. N. BONORA, *Identification and measurement of ductile damage parameters*, J. of Strain Analysis, **34**, 463–478 1999.
8. S. DHAR, *et al.*, *A continuum damage mechanics model for ductile fracture*, International Journal of Pressure Vessels and Piping, **77**, 335–344, 2000.

9. J.S. VETRANO, *et al.*, *Evidence for excess vacancies at sliding grain boundaries during superplastic deformation*, Acta Materialia, **47**, 4125–4129, 1999.
10. M.A. KHALEEL, *et al.*, *Constitutive modeling of deformation and damage in superplastic materials*, International J. of Plasticity, **17**, 277–296, 2001.
11. D.R. HAYHURST, *Creep rupture under multi-axial states of stress*, J. Mech. Phys. Solids, **20**, 381–390, 1972.
12. J. LIN and Y. LIU, *A set of unified constitutive equations for modelling microstructure evolution in hot deformation*, J. of Materials Processing Technology, **143–144**, 281–285, 2003.
13. L.G. LIM and F.P.E. DUNNE, *Modelling central bursting in the extrusion of particulate reinforced metal matrix composite materials*, Int. J. of Machine Tools and Manufacture, **37**, 901–915, 1997.
14. A.A. HOWE, D.C.J. FARRUGIA, *Alloy design: from composition to through process models*, Materials Science and Technology, **15**, 15–21, 1999.
15. J. LIN, F.P.E. DUNNE and D.R. HAYHURST, *Physically-based temperature dependence of elastic viscoplastic constitutive equations for copper between 20 and 500 °C*, Philosophical Magazine, A, **74**, 2, 655–676, 1996.
16. B. LI, J. LIN, and X. YAO, *A novel evolutionary algorithm for determining unified creep damage constitutive equations*, Int. J. of Mech. Sci., **44**, 5, 987–1002, 2002.
17. J. LIN, B.H. CHEONG, and X. YAO, *Universal multi-objective function for optimising superplastic-damage constitutive equations*, J. of Mat. Proc. Tech., **125–126**, 199–205, 2002.

Received August 18, 2005; revised version January 16, 2006.
